Hindawi
Journal of Function Spaces
Volume 2020, Article ID 8898309, 17 pages
https://doi.org/10.1155/2020/8898309

Research Article

Meshless Technique for the Solution of Time-Fractional Partial Differential Equations Having Real-World Applications

Mehnaz Shakeel,[1,2] Iltaf Hussain,[1] Hijaz Ahmad,[1,3] Imtiaz Ahmad,[4] Phatiphat Thounthong,[5] and Ying-Fang Zhang[6]

[1]*Department of Basic Sciences, University of Engineering and Technology, Peshawar, Pakistan*
[2]*Department of Mathematics, Shaheed Benazir Bhutto Women University, Peshawar, Pakistan*
[3]*Section of Mathematics, International Telematic University Uninettuno, Corso Vittorio Emanuele II, 39, 00186 Roma, Italy*
[4]*Department of Mathematics, University of Swabi, Khyber Pakhtunkhwa, Pakistan*
[5]*Renewable Energy Research Centre, Department of Teacher Training in Electrical Engineering, Faculty of Technical Education, King Mongkut's University of Technology North Bangkok, 1518 Pracharat 1 Road, Bangsue, Bangkok 10800, Thailand*
[6]*School of Mathematics and Information Science, Henan Polytechnic University, Jiaozuo 454000, China*

Correspondence should be addressed to Ying-Fang Zhang; zhangyingfang@hpu.edu.cn

Received 16 September 2020; Revised 2 October 2020; Accepted 7 October 2020; Published 24 October 2020

Academic Editor: Kottakkaran Sooppy Nisar

In this article, radial basis function collocation scheme is adopted for the numerical solution of fractional partial differential equations. This method is highly demanding because of its meshless nature and ease of implementation in high dimensions and complex geometries. Time derivative is approximated by Caputo derivative for the values of $\alpha \in (0, 1)$ and $\alpha \in (1, 2)$. Forward difference scheme is applied to approximate the 1^{st} order derivative appearing in the definition of Caputo derivative for $\alpha \in (0, 1)$, whereas central difference scheme is used for the 2^{nd} order derivative in the definition of Caputo derivative for $\alpha \in (1, 2)$. Numerical problems are given to judge the behaviour of the proposed method for both the cases of α. Error norms are used to asses the accuracy of the method. Both uniform and nonuniform nodes are considered. Numerical simulation is carried out for irregular domain as well. Results are also compared with the existing methods in the literature.

1. Introduction

Fractional order calculus is a dynamic branch of calculus, which is concerned with the integration and differentiation of noninteger order. This branch of mathematics attracted researchers in the last few decades [1–7]. Fractional partial differential equations (FPDEs) are commonly used to model problems in the field of science, engineering, and many other fields including fluid mechanics, chemistry, viscoelasticity, finance, and physics. Some interesting applications of FPDEs can be found in [8–11]. Many researchers did considerable work to find the analytic solution of FPDEs [12–14], but it is difficult and sometimes impossible to find the analytic solution of most of FPDEs. Therefore, many researchers referred to numerical techniques to find the solution of FPDEs [15–20]. There are two widely used definitions of fractional derivatives, namely, Caputo and Riemann-Liouville. The main difference between these two operators is the order of evaluation. Many authors analyzed time-fractional partial differential equations (PDEs), for example, Wyss [14], Agrawal [21], Liu et al. [22], Jiang and Ma. [23], and Chang et al. [24].

Radial basis function (RBF) method has been used to find the solution of FPDEs. RBF collocation schemes are used to find the solution of PDEs, integral equations, integrodifferential equation, etc. The main idea behind the RBF method is to approximate space derivatives by RBFs which converts PDE to a system of linear equations. The solution of this system of linear equations leads to the solution of governing equation. This method is getting fame due to its meshless nature and easy to use in high dimensions and complex geometries. To utilize this advantage of RBF scheme, it is applied to time-

fractional PDEs for higher dimensions and with different types of domains. In this paper, implicit scheme (IS) and Crank-Nicolson scheme (CNS) are coupled with RBF. Many authors used meshless RBF method to solve FPDEs [25–35]. In this paper, multiquadric (MQ) RBF is used to approximate solution. MQ-RBF is defined by

$$\varphi(r_{ij}) = \sqrt{r_{ij}^2 + c^2}, \tag{1}$$

where $r_{ij} = \|\mathbf{z}_i - \mathbf{z}_j\|$, $i, j = 1, 2, \cdots, N$, N is the number of collocation points and c is the shape parameter. Furthermore, $\mathbf{z} = z_1$ in one dimensional, and $\mathbf{z} = (z_1, z_2)$ in two-dimensional case.

Kansa [36] has applied the multiquadric radial basis function (MQ-RBF) collocation method to solve PDEs. After that, there are a lot of applications and developments of the MQ-RBF as an efficient meshless method to solve engineering problems. However, the ill-conditioned behaviour and the sensitivity to the shape parameter are the main obstacles in the Kansa's MQ-RBF method. Many researchers have discussed the optimal shape parameter used in the MQ-RBF [37–39]. Formulation of the method flows in the following major steps:

(1) Approximate time-fractional derivative by using Caputo definition

(2) Approximate the space variable by RBFs

(3) Substitute the values obtained from the previous two steps in the problem to get a system of linear equations

$$\frac{\partial^\alpha \nu}{\partial t^\alpha} = \begin{cases} \dfrac{1}{\Gamma(1-\alpha)} \displaystyle\int_0^t \frac{\partial^{\eta+1}\nu}{\partial t^{\eta+1}} (t-\tau)^{\eta-\alpha} d\tau, \eta < \alpha < \eta + 1, \\ \dfrac{\partial^{\eta+1}\nu}{\partial t^{\eta+1}}, \alpha = \eta + 1. \end{cases} \tag{2}$$

Definition 1. Caputo derivative of noninteger order α of a function $\nu(\mathbf{z}, t)$ is defined by [9]

In this paper, we have tackled the following two cases of Caputo derivative:

Case I. $0 < \alpha < 1$

Case II. $1 < \alpha < 2$

1.1. Governing Equation. We emphasize on the following time-fractional PDE

$$\frac{\partial^\alpha \nu}{\partial t^\alpha} + \mathfrak{L}(\nu) = \psi(\mathbf{z}, t), \mathbf{z} \in \Omega, \eta < \alpha < \eta + 1, t > 0. \tag{3}$$

The boundary conditions (BCs) are

$$\nu(\mathbf{z}, t) = G(\mathbf{z}, t), \mathbf{z} \in \partial\Omega, t > 0, \tag{4}$$

and the initial conditions (ICs) are

$$\nu(\mathbf{z}, 0) = \mu(\mathbf{z}), \nu_t(\mathbf{z}, 0) = \nu(\mathbf{z}), \tag{5}$$

where $\nu(\mathbf{z}, t)$ is the solution, $\partial^\alpha \nu / \partial t^\alpha$ is the Caputo fractional derivative of order α, $\psi(\mathbf{z}, t)$ is the source term, Ω is the bounded domain, and $\partial\Omega$ is the boundary. Equation (3) can be fractional diffusion, fractional wave diffusion, or fraction anomalous diffusion equation depending on $\mathfrak{L}(\nu)$. Here, $\mathfrak{L}(\nu)$ is a linear operator defined by

$$\mathfrak{L}(\nu) = \mathfrak{a}\Delta\nu + \mathfrak{b}\nabla\nu + \mathfrak{c}\nu, \tag{6}$$

where $\mathfrak{a}$, $\mathfrak{b}$, and $\mathfrak{c}$ are functions of $\mathbf{z}$ or constants and Δ and ∇ denote Laplacian and gradient operator, respectively.

1.2. Main Objective of the Paper. This paper is aimed at solving FPDEs by using the combination of Caputo fractional derivative operator and RBFs. Caputo fractional derivative operator is applied to approximate the time derivative whereas RBFs are adopted to approximate the space derivatives. The organization of the rest of the paper is as follows: Section 2 is dedicated to construct meshless scheme for the first case, i.e., $0 < \alpha < 1$. In Section 3, we consider the second case, i.e., $1 < \alpha < 2$. In section 4, the numerical method is applied to different problems and comparison is made with some other methods. Section 5 is authoritative to give the concluding note of this work.

2. Formulation of the Method for Case I

In this section, we take $0 < \alpha < 1$ and find $\partial^\alpha \nu / \partial t^\alpha$, by using Caputo derivative. Finite difference scheme is applied to approximate the 1st order time derivative appearing on the right-hand side of Caputo derivative. Then, θ-weighted scheme is applied to the governing equation, and the value of the time derivative is also substituted.

2.1. Time-Fractional Derivative. Caputo fractional derivative for $\alpha \in (0, 1)$ is defined by

$$\frac{\partial^\alpha \nu}{\partial t^\alpha} = \begin{cases} \dfrac{1}{\Gamma(1-\alpha)} \displaystyle\int_0^t \frac{\partial \nu}{\partial t} (t-\tau)^{-\alpha} d\tau, 0 < \alpha < 1, \\ \dfrac{\partial \nu}{\partial t}, \alpha = 1. \end{cases} \tag{7}$$

Taking derivative at $t = t^{n+1}$, we get

$$\frac{\partial^\alpha \nu(\mathbf{z}, t^{n+1})}{\partial t^\alpha} = \frac{1}{\Gamma(1-\alpha)} \int_0^{t^{n+1}} \frac{\partial \nu}{\partial t} \left(t^{n+1} - \tau\right)^{-\alpha} d\tau. \tag{8}$$

This implies

$$\frac{\partial^\alpha \nu}{\partial t^\alpha} = \frac{1}{\Gamma(1-\alpha)} \sum_{k=0}^{n} \int_{t^k}^{t^{k+1}} \frac{\partial \nu}{\partial t} \left(t^{n+1} - \tau\right)^{-\alpha} d\tau. \tag{9}$$

Now, we use finite difference scheme to approximate $\partial^{n+1}\nu / \partial t^{n+1}$, as follows:

$$\frac{\partial v}{\partial t} = \frac{v^{k+1} - v^k}{dt} + o(dt), \tag{10}$$

where dt is the time step size.

Then

$$\begin{aligned}\frac{\partial^\alpha v(\mathbf{z}, t^{n+1})}{\partial t^\alpha} &\approx \frac{1}{\Gamma(1-\alpha)} \sum_{k=0}^{n} \int_{t^k}^{t^{k+1}} \left(\frac{v^{k+1} - v^k}{dt} + o(dt)\right) \\ &\quad \cdot \left(t^{n+1} - \tau\right)^{-\alpha} d\tau, \frac{\partial^\alpha v}{\partial t^\alpha} \\ &= a_\alpha \sum_{k=0}^{n} b_k \left(v^{n-k+1} - v^{n-k}\right) + \left(o(dt)^{2-\alpha}\right),\end{aligned} \tag{11}$$

where $a_\alpha = dt^{-\alpha}/\Gamma(2-\alpha)$ and $b_k = (k+1)^{1-\alpha} - k^{1-\alpha}$, $k = 0, 1, \cdots, n$.

Finally, we can write in more precise form as

$$\frac{\partial^\alpha v}{\partial t^\alpha} = \begin{cases} a_\alpha \left(v^{n+1} - v^n\right) + a_\alpha \sum_{k=1}^{n} b_k \left(v^{n-k+1} - v^{n-k}\right), n \geq 1, \\ a_\alpha \left(v^1 - v^0\right), n = 0. \end{cases} \tag{12}$$

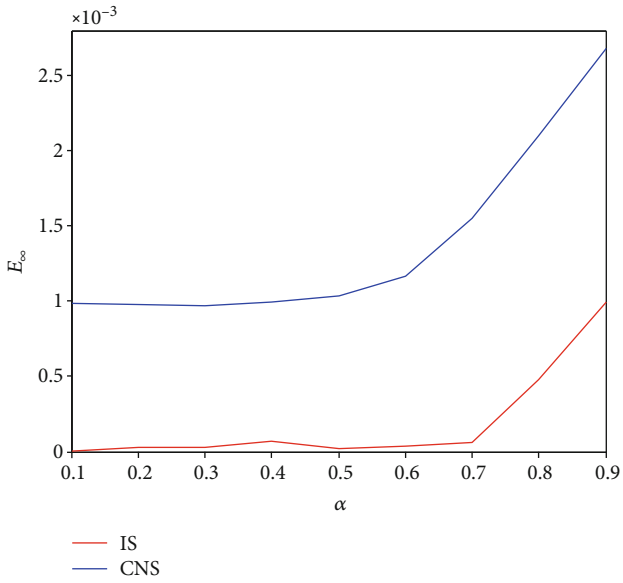

Figure 1: Comparison of E_∞ of IS and CNS for the Problem 3.

2.2. θ-Weighted Scheme. Applying θ-weighted scheme to Eq. (3) and substituting Eq. (12) in Eq. (3), we get

$$a_\alpha v^{n+1} + \theta \mathfrak{L}\left(v^{n+1}\right) = \begin{cases} a_\alpha v^n - (1-\theta)\mathfrak{L}(v^n) - a_\alpha \sum_{k=1}^{n} b_k \left(v^{n-k+1} - v^{n-k}\right) + \psi^{n+1}, n \geq 1, \\ a_\alpha v^0 - (1-\theta)\mathfrak{L}\left(v^0\right) + \psi^1, n = 0. \end{cases} \tag{13}$$

Now, we employ Kansa's method and interpolate $v(\mathbf{z}, t^{n+1})$ by RBFs. We interpolate the solution at N different points $\mathbf{z}_i \mid i = 1, 2, \cdots, N$, where $\mathbf{z}_i \mid i \in \Omega$ are interior points while $\mathbf{z}_1$ and $\mathbf{z}_N$ are boundary points.

$$\begin{aligned} v\left(\mathbf{z}, t^{n+1}\right) &= \sum_{i=1}^{N} \lambda_i^{n+1} \varphi\left(\|\mathbf{z}_i - \mathbf{z}_j\|\right), j = 1, 2, \cdots, N \\ &= \sum_{i=1}^{N} \lambda_i^{n+1} \varphi\left(r_{ij}\right), \end{aligned} \tag{14}$$

where $\varphi(r_{ij})$ are the RBFs, $\|.\|$ is Euclidian norm, and λ_i's are the unknown constants.

We can write Eq. (14) in matrix form as

$$v^{n+1} = \mathbf{A}\lambda^{n+1} \tag{15}$$

or

$$\lambda^{n+1} = \mathbf{A}^{-1} v^{n+1}. \tag{16}$$

Provided that collocation matrix $\mathbf{A}$ must be nonsingular to ensure the invertibility of matrix $\mathbf{A}$. This depends on the choice of RBF and the location of mesh points. Matrix $\mathbf{A}$ is invertible for distinct mesh points. The shape parameter has an important effect on condition number [40]. Once we find the constants λ_i^{n+1}, we can find solution v from Eq. (14).

Putting the value from Eq. (15) in Eq. (13), we get the following form

$$a_\alpha \mathbf{A}\lambda^{n+1} + \theta \mathfrak{L}\left(\mathbf{A}\lambda^{n+1}\right) = \begin{cases} a_\alpha \mathbf{A}\lambda^n - (1-\theta)\mathfrak{L}(\mathbf{A}\lambda^n) - a_\alpha \sum_{k=1}^{n} b_k \left(v^{n-k+1} - v^{n-k}\right) + \psi^{n+1}, & n \geq 1, \\ a_\alpha \mathbf{A}\lambda^0 - (1-\theta)\mathfrak{L}\left(\mathbf{A}\lambda^0\right) + \psi^1, & n = 0. \end{cases} \tag{17}$$

$$\lambda^{n+1} = \mathbb{M}^{-1}\mathbb{N}\lambda^n + \mathbb{M}^{-1}\mathbb{G}^{n+1}, n \geq 0, \tag{18}$$

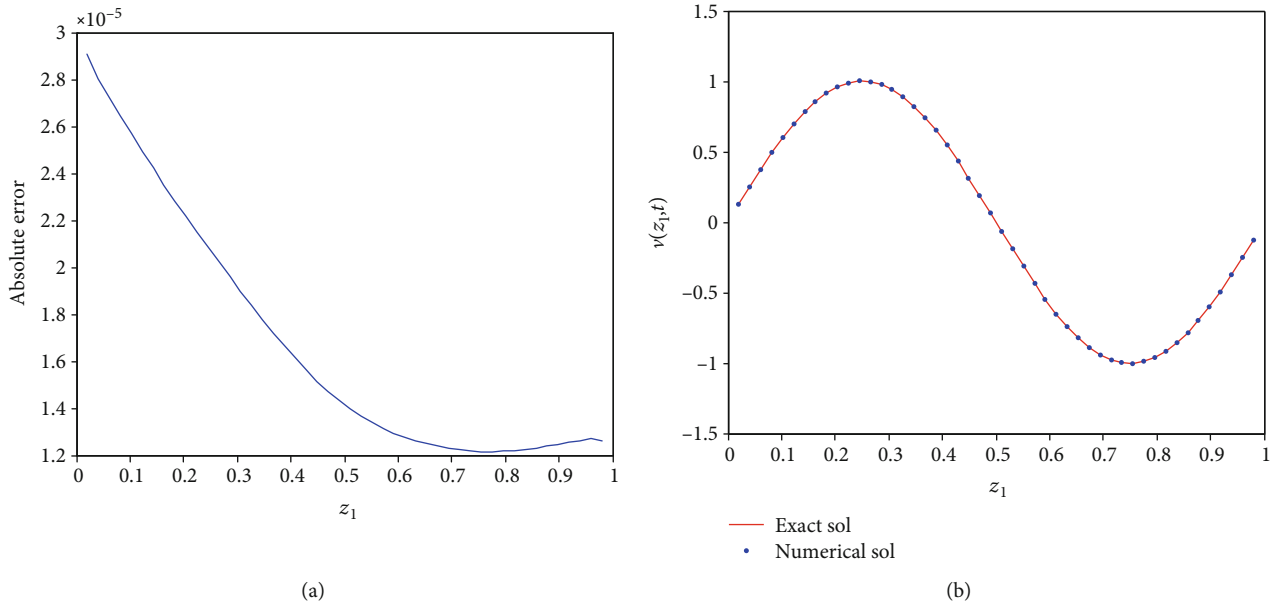

FIGURE 2: (a) E_{abs} and (b) exact and approximate solution at $\alpha = 0.2$ for the Problem 3.

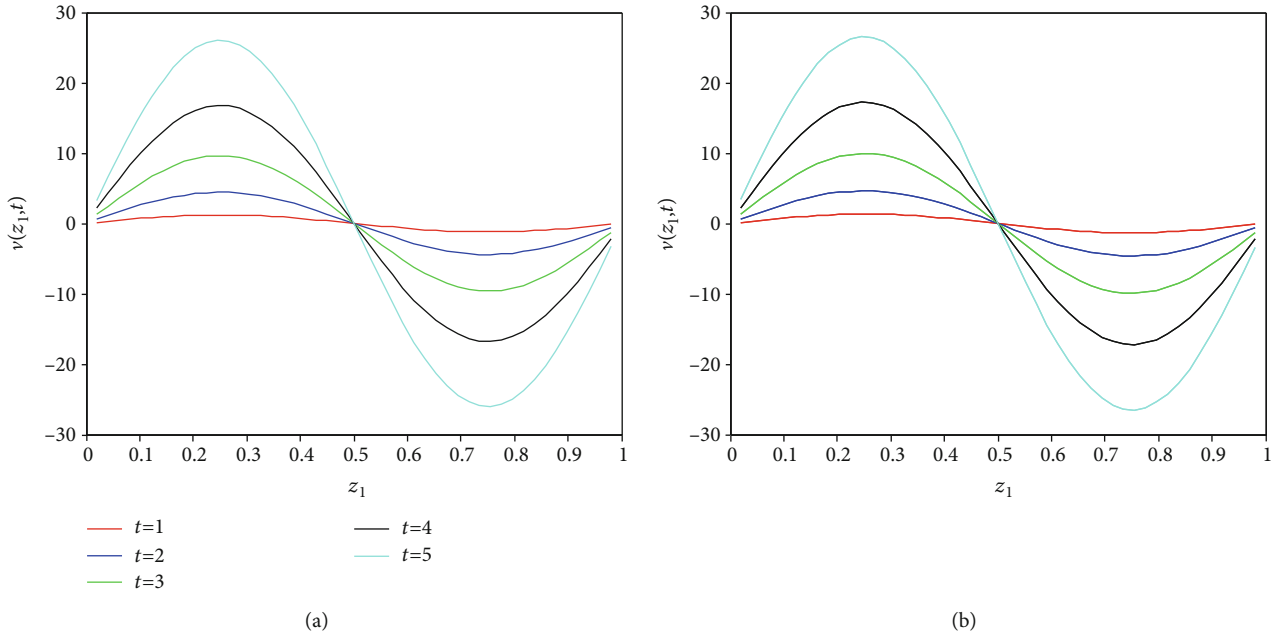

FIGURE 3: Approximate solution at different time levels by using (a) IS and (b) CNS for the Problem 3.

where

$$\mathbf{M} = a_\alpha \mathbf{A} + \theta \mathfrak{L}(\mathbf{A}), \mathbf{N} = a_\alpha \mathbf{A} - (1-\theta)\mathfrak{L}(\mathbf{A}),$$

$$\mathbf{M}\mathbf{G}^{n+1} = \begin{cases} \mathbf{G}_1^{n+1} + \mathbf{G}_2^{n+1}, & n \geq 1, \\ \psi^1, & n = 0. \end{cases} \tag{19}$$

Here,

$$\mathbf{G}_1^{n+1} = \left\{ g_1^{n+1}, 0, \cdots, g_2^{n+1} \right\},$$

$$\mathbf{G}_2^{n+1} = -a_\alpha \sum_{k=1}^{n} b_k \left(v^{n-k+1} - v^{n-k} \right) + \psi^{n+1}, \tag{20}$$

where g_1^{n+1} and g_2^{n+1} are some known functions given in BCs. Finally, from Eq. (18) and Eq. (16), we get

$$\mathbf{v}^{n+1} = \mathbf{A}\mathbf{M}^{-1}\mathbf{N}\mathbf{A}^{-1}\mathbf{v}^n + \mathbf{A}\mathbf{M}^{-1}\mathbf{G}^{n+1}. \tag{21}$$

We can use this scheme to find the solution at any time level t^n.

2.3. Stability and Convergence. The scheme (21) is basically a recurrence relation which gives the values of solution at the time t^{n+1} by using solution at time t^n. The matrix $E = \mathbf{A}\mathbf{M}^{-1}\mathbf{N}\mathbf{A}^{-1}$ is known as amplification matrix, and the elements of

this matrix depend on the constant $\kappa = dt/h^{\varsigma}$, where dt is the time step, h is the distance between any two successive nodes, and ς is the order of spatial differential operator. Let us denote the exact solution of Eq. (3) by v^n at time t^n.

We state a well-known theorem of Fasshauer [41] (see [42] for proof):

$$\left|D^{\alpha}f(\mathbf{z}) - \mathrm{D}^{\alpha}P_f(\mathbf{z})\right| \le Ch_{\chi,\Omega}^{k-|\alpha|}\sqrt{C_{\Phi}(x)}\left|f_{\mathcal{N}_{\phi}(\Omega)}\right|, \tag{22}$$

provided that $h_{\chi,\Omega} \le h_0$. Here,

$$C_{\Phi}(\mathbf{z}) = \max_{\substack{\beta,\gamma\in\mathbb{N}_0^s \\ |\beta|+|\gamma|=2k}} \max_{w,z\in\Omega\cap B(x,c_2h\chi,\Omega)} \left|D_1^{\beta}D_2^{\gamma}\Phi(w,z)\right|. \tag{23}$$

Theorem 2. *[41] Suppose $\Omega \subseteq \mathbb{R}^s$ is open and bounded and satisfies an interior cone condition. Suppose $\Phi \in C^{2k}(\Omega\times\Omega)$ is symmetric and strictly conditionally positive definite of order m on $\mathbb{R}^s$. Denote the interpolant to $f \in \mathcal{N}_{\phi}(\Omega)$ on the $(m-1)$ -unisolvent set χ by P_f . Fix $\alpha \in \mathbb{N}_0^s$ with $|\alpha| \le k$. Then, there exist positive constants h_0 and C (independent of $\boldsymbol{z}$, f, and Φ) such that*

Application of Theorem 2 to infinitely smooth functions such as Gaussians or generalized (inverse) multiquadrics immediately yield arbitrarily high algebraic convergence rates, i.e., for every $k \in \mathbb{N}$ and $|\alpha| \le k$, we have

$$\left|D^{\alpha}f(\mathbf{z}) - D^{\alpha}P_f(\mathbf{z})\right| \le C_k h^{k-|\alpha|}\left|v_{\mathcal{N}_{\phi}(\Omega)}\right|, \tag{24}$$

whenever $f \in \mathcal{N}_{\phi}(\Omega)$ and $\mathcal{N}_{\phi}(\Omega)$ represent the native space of RBFs. A considerable amount of work has gone into investigating the dependence of the constant C_k on k [43].

In this work, MQ-RBF is used, so it is concluded that

$$|D^{\alpha}\widehat{v}(\mathbf{z}) - D^{\alpha}v(\mathbf{z})| \le C_k h^{k-|\alpha|}\left|v_{\mathcal{N}_{\phi}(\Omega)}\right|, \tag{25}$$

where $\widehat{v}$ and v are the exact and approximate solution, respectively. Now let us assume that the scheme (21) is p^{th} order accurate in space, then

$$v^{n+1} = Ev^n + \mathbf{A}\mathbf{M}^{-1}\mathbf{G}^{n+1} + o\left((dt)^{2-\alpha} + h^p\right), dt, h \to 0. \tag{26}$$

Let us define the residual by $\varepsilon^n = v\wedge^n - v^n$, then

$$\varepsilon^{n+1} = E\varepsilon^n + o\left((dt)^{2-\alpha} + h^p\right), dt, h \to 0. \tag{27}$$

By Lax-Richtmyer definition of stability, the scheme (21) is stable if

$$\|E\| \le 1, \tag{28}$$

Table 1: Error norms and computational order for different values of dt with $c = 5.1$, $N = 50$ for the Problem 3.

θ	dt	E_{∞}	E_{RMS}	C_1-order
1	0.1	3.2163*e*-05	1.7837*e*-05	—
	0.05	2.6247*e*-05	1.0503*e*-05	0.2932
	0.01	1.4223*e*-05	1.1387*e*-05	0.3807
	0.005	6.7040*e*-06	3.0043*e*-06	1.0851
	0.001	4.0082*e*-06	1.7611*e*-06	0.3196
$\frac{1}{2}$	0.1	1.0700*e*-01	7.4900*e*-02	—
	0.05	5.1100*e*-02	3.5800*e*-02	1.0662
	0.01	9.8000*e*-03	6.9000*e*-03	1.0261
	0.005	4.9000*e*-03	3.4000*e*-03	1.0000
	0.001	9.8295*e*-04	6.8233*e*-04	0.9981

Table 2: Error norms for different values of α for the Problem 3.

α	IS		CNS	
	E_{∞}	E_{RMS}	E_{∞}	E_{RMS}
0.2	7.7846*e*-05	4.7558*e*-05	1.0700*e*-01	7.4900*e*-02
0.4	2.2439*e*-04	1.4815*e*-04	1.0710*e*-01	7.5000*e*-02
0.6	5.5165*e*-04	3.8107*e*-04	1.0750*e*-01	7.5300*e*-02
0.8	1.2000*e*-03	8.3507*e*-04	1.0830*e*-01	7.5900*e*-02

Table 3: Comparison with of E_{∞} [35] for the Problem 4.

α	IS	CNS	[35]
0.20	2.0316*e*-06	3.9338*e*-06	2.3228*e*-05
0.50	9.9440*e*-07	3.6707*e*-06	1.9343*e*-05
0.75	2.3590*e*-06	1.6847*e*-06	1.4279*e*-05
0.90	7.3325*e*-06	7.9323*e*-06	8.4900*e*-06

when matrix E is normal then $\|E\| = \rho(E)$; otherwise, the inequality $\rho(E) \le \|E\|$ is always true. It is assumed that the step size h is to be small enough, and the solution and IC of the given problem must be sufficiently smooth. We must have $dt \to 0$ to keep $\kappa = dt/h^p$ constant. Therefore, there exist some constant C such that

$$\left\|\varepsilon^{n+1}\right\| \le \|E\|\|\varepsilon^n\| + C\left((dt)^{2-\alpha} + h^p\right), n = 0, 1, 2, \cdots, T\times M. \tag{29}$$

Since the residual ε^n obeys zero IC and BCs, so $\varepsilon^0 = 0$. So by mathematical induction, we have

$$\left\|\varepsilon^{n+1}\right\| \le \left(1 + \|E\|^2 + \|E\|^3 + \cdots + \|E\|^{n-1}\right)C\left((dt)^{2-\alpha} + h^p\right), \quad n = 0, 1, 2, \cdots, T\times M. \tag{30}$$

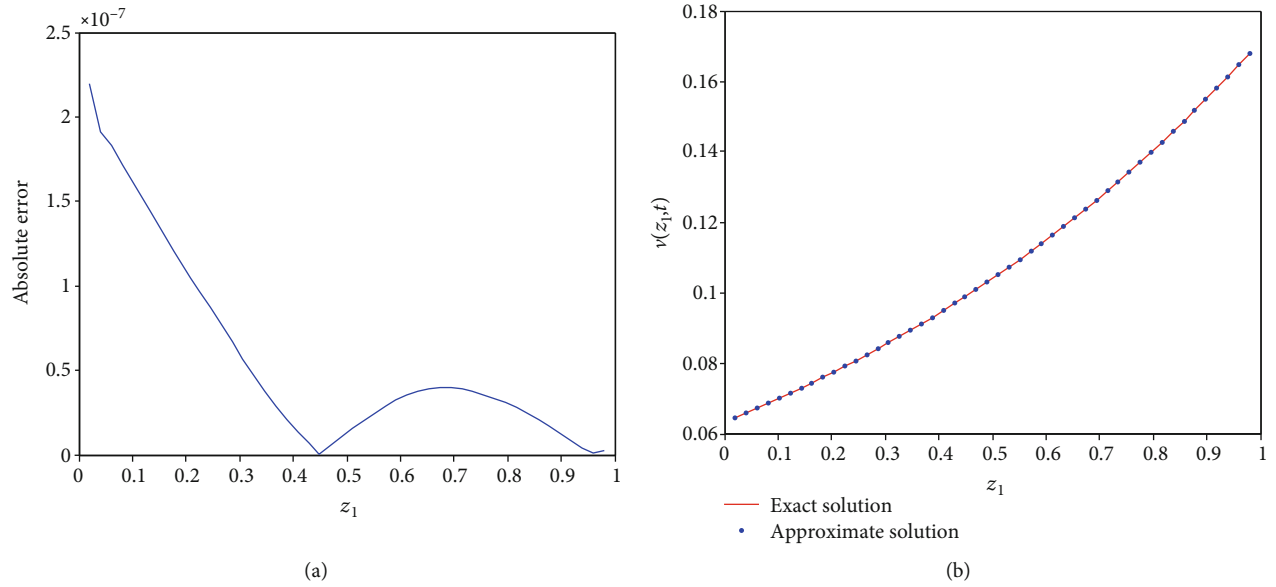

FIGURE 4: (a) E_{abs} and (b) exact and approximate solution at $\alpha = 0.2$ for the Problem 4.

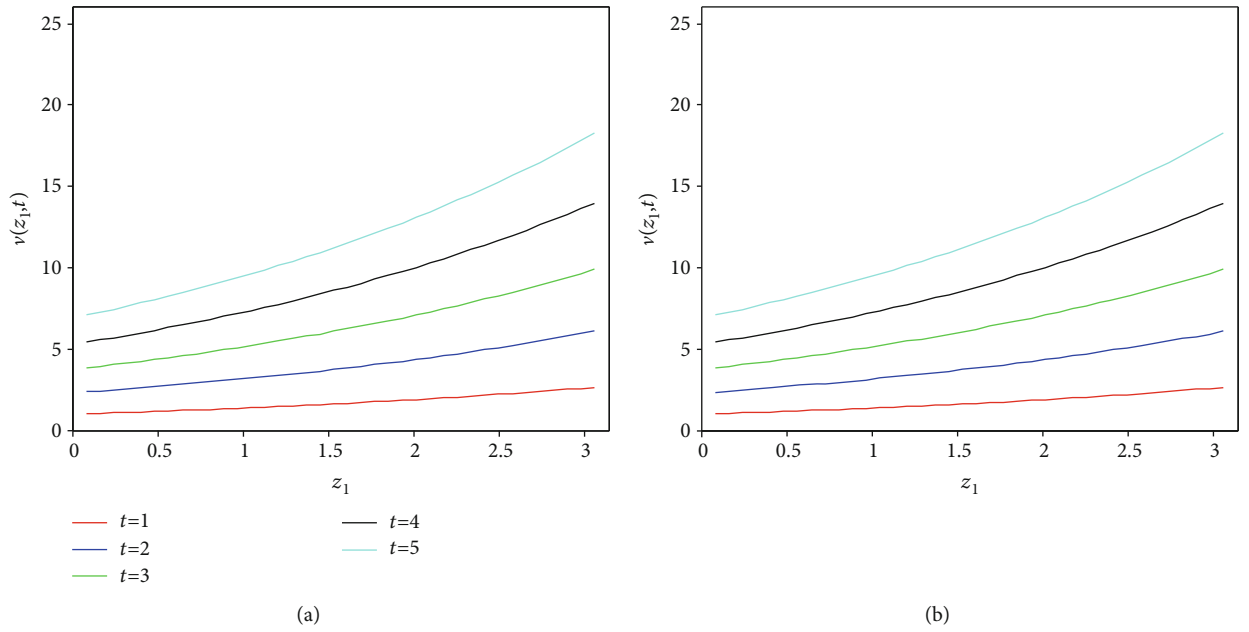

FIGURE 5: Approximate solution at different time levels by using (a) IS and (b) CNS for the Problem 4.

Using the condition given in Eq. (28), we have

$$\left\|\varepsilon^{n+1}\right\| \le nC\left((dt)^{2-\alpha} + h^p\right), n = 0, 1, 2, \cdots, T \times M. \quad (31)$$

Hence, the scheme is convergent.

3. Formulation of the Method for Case II

In this section, we take $1 < \alpha < 2$ and find $\partial^\alpha v/\partial t^\alpha$ by using Caputo derivative. We approximate the 2nd order time derivative (appearing in the Caputo derivative) by the central difference scheme. We then apply θ-weighted scheme to the governing equation.

3.1. Time-Fractional Derivative. Caputo fractional derivative for $\alpha \in (1, 2)$ is defined by

$$\frac{\partial^\alpha v}{\partial t^\alpha} = \begin{cases} \dfrac{1}{\Gamma(2-\alpha)} \displaystyle\int_0^t \frac{\partial^2 v}{\partial t^2} (t-\tau)^{1-\alpha} d\tau, & 1 < \alpha < 2, \\ \dfrac{\partial^2 v}{\partial t^2}, & \alpha = 2. \end{cases} \quad (32)$$

Taking derivative at $t = t^{n+1}$, we get

$$\frac{\partial^\alpha v\left(\mathbf{z}, t^{n+1}\right)}{\partial t^\alpha} = \frac{1}{\Gamma(2-\alpha)} \int_0^{t^{n+1}} \frac{\partial^2 v}{\partial t^2} \left(t^{n+1} - \tau\right)^{1-\alpha} d\tau. \quad (33)$$

Table 4: Error norms and computational order for different time steps with $c = 5.1$, $N = 50$ and $t = 1$ for the Problem 4.

θ	dt	E_∞	E_{RMS}	$C_1 - order$
1	0.1	1.2261*e*-04	9.3157*e*-05	–
	0.05	1.9822*e*-05	1.5126*e*-05	2.6289
	0.01	6.4769*e*-06	2.8484*e*-06	0.6950
	0.005	4.0646*e*-06	2.2878*e*-06	0.6722
	0.001	2.0397*e*-06	8.3217*e*-07	0.4284
$\frac{1}{2}$	0.1	1.1200*e*-02	8.5000*e*-03	–
	0.05	5.1000*e*-03	3.9000*e*-0	1.1350
	0.01	1.1000*e*-03	7.6660*e*-04	0.9527
	0.005	5.3126*e*-04	3.8540*e*-04	1.0500
	0.001	1.0499*e*-04	7.7472*e*-05	0.9756

This implies

$$\frac{\partial^\alpha v}{\partial t^\alpha} = \frac{1}{\Gamma(2-\alpha)} \sum_{k=0}^{n} \int_{t^k}^{t^{k+1}} \frac{\partial^2 v}{\partial t^2} \left(t^{n+1} - \tau\right)^{1-\alpha} d\tau. \tag{34}$$

Now, we approximate $\partial^2 v/\partial t^2$ by finite difference scheme, as follows:

$$\frac{\partial^2 v(\mathbf{z}, \tau^{k+1})}{\partial \tau^2} = \frac{v^{k+1} - 2v^k + v^{k-1}}{dt^2} + o(dt)^2. \tag{35}$$

Repeating the same process as we did in Section 2.1,

Table 5: Comparison with of E_∞ [44] for the Problem 3.

α	IS	CNS	[44]
0.20	3.3143*e*-07	5.5885*e*-06	2.6640*e*-05
0.50	2.9331*e*-07	2.5374*e*-06	8.1200*e*-06
0.75	1.0587*e*-06	2.9157*e*-06	9.5300*e*-06
0.90	5.4445*e*-06	3.9059*e*-06	4.3240*e*-05

we get

$$\frac{\partial^\alpha v}{\partial t^\alpha} = a_\alpha \left(v^{n+1} - 2v^n + v^{n-1}\right) + a_\alpha \sum_{k=1}^{n} b_k \left(v^{n-k+1} - 2v^{n-k} + v^{n-k-1}\right) + o\left(dt^{(3-\alpha)}\right), n \geq 0, \tag{36}$$

where $a_\alpha = dt^{-\alpha}/\Gamma(3-\alpha)$ and $b_k = (k+1)^{2-\alpha} - k^{2-\alpha}$,$k = 0, 1, \cdots, n$.

Now there exist v^{-1} for $n = 0$ and $k = n$, for which we use the second IC, i.e.,

$$\begin{aligned} v_t^0 &= \frac{v^1 - v^{-1}}{2dt}, \\ v^{-1} &= v^1 - 2dt v_t^0. \end{aligned} \tag{37}$$

Hence, we get the following value of $\partial^\alpha v/\partial t^\alpha$,

$$\frac{\partial^\alpha v}{\partial t^\alpha} = \begin{cases} a_\alpha \left(v^{n+1} - 2v^n + v^{n-1}\right) + a_\alpha \sum_{k=1}^{n-1} b_k \left(v^{n-k+1} - 2v^{n-k} + v^{n-k-1}\right) + 2a_\alpha b_n \left(v^1 - v^0 - dt v_t^0\right), & n \geq 1 \\ , & \\ 2a_\alpha \left(v^1 - v^0 - dt v_t^0\right), & n = 0. \end{cases} \tag{38}$$

3.2. θ-Weighted Scheme. Applying θ-weighted scheme to Eq. (3) and substituting Eq. (38) in Eq. (3), we get the following scheme for $n = 0$ and $n \geq 1$, respectively.

$$2a_\alpha v^1 + \theta \mathfrak{L}\left(v^1\right) = 2a_\alpha v^0 + 2a_\alpha dt v_t^0 - (1-\theta)\mathfrak{L}\left(v^0\right) + \psi^1, n = 0 \tag{39}$$

$$\begin{aligned} a_\alpha v^{n+1} + \theta \mathfrak{L}\left(v^{n+1}\right) = {} & 2a_\alpha v^n - a_\alpha v^{n-1} - 2a_\alpha b_n \left(v^1 - v^0 - dt v_t^0\right) \\ & - a_\alpha \sum_{k=1}^{n-1} b_k \left(v^{n-k+1} - 2v^{n-k} + v^{n-k-1}\right) \\ & - (1-\theta)\mathfrak{L}(v^n) + \psi^{n+1}, n \geq 1. \end{aligned} \tag{40}$$

Proceeding in the same way as in the Section 2.2, we get $\mathbf{v}^1$ and $\mathbf{v}^{n+1}$, respectively,

$$\mathbf{v}^1 = \mathbf{A}\mathbb{M}^{-1}\mathbb{N}\mathbf{A}^{-1}\mathbf{v}^0 + \mathbf{A}\mathbb{M}^{-1}\mathbb{H}, \tag{41}$$

where

$$\begin{aligned} \mathbb{M} &= 2a_\alpha \mathbf{A} + \theta \mathfrak{L}(\mathbf{A}), \\ \mathbb{N} &= 2a_\alpha \mathbf{A} - (1-\theta)\mathfrak{L}(\mathbf{A}), \\ \mathbb{H} &= \mathbb{H}_1 + \mathbb{H}_2, \\ \mathbb{H}_1 &= \{g_1, 0, \cdots, g_2\}, \\ \mathbb{H}_2 &= \psi^1 + 2a_\alpha dt v_t^0. \end{aligned} \tag{42}$$

Also,

$$\mathbf{v}^{n+1} = \mathbf{A}\mathbb{M}_1^{-1}\mathbb{N}\mathbf{A}^{-1}\mathbf{v}^n + \mathbf{A}\mathbb{M}_1^{-1}\mathbb{P}\mathbf{A}^{-1}\mathbf{v}^{n-1} + \mathbf{A}\mathbb{M}_1^{-1}\mathbb{G}^{n+1}, n \geq 1, \tag{43}$$

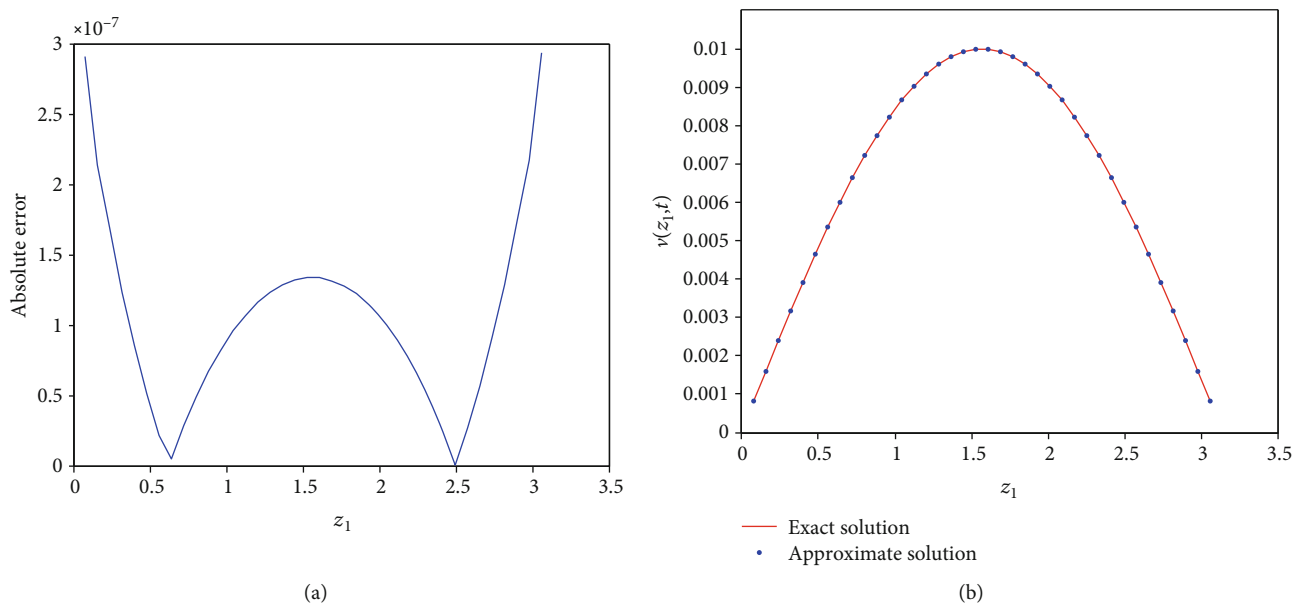

Figure 6: (a) E_{abs} and (b) exact and approximate solution for $\alpha = 0.50$ for the Problem 5.

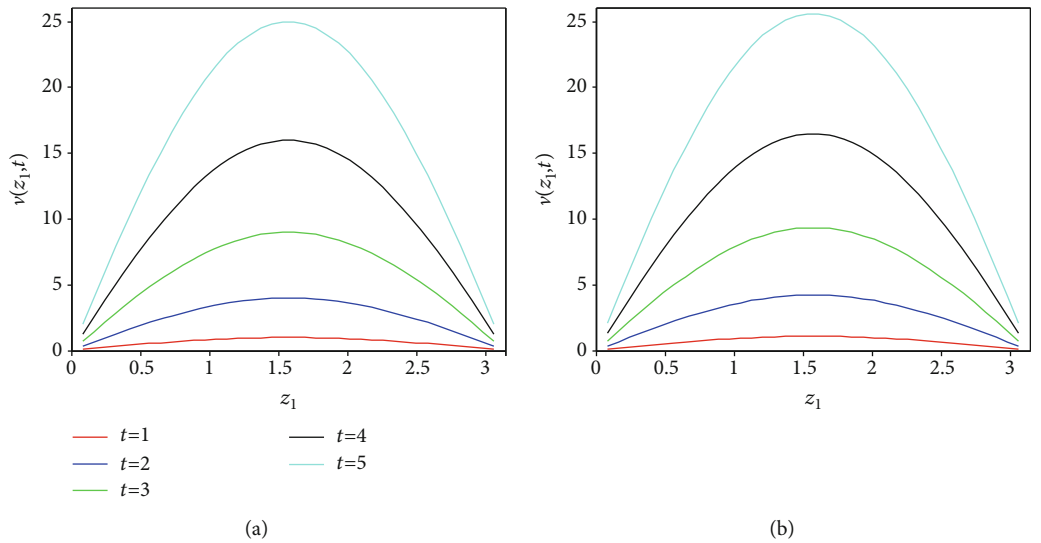

Figure 7: Approximate solution at different time levels by using (a) IS and (b) CNS for the Problem 3.

Table 6: Error norms and computational order for different time steps for $N = 50$, $c = 8.1$ and $t = 1$ for the Problem 3.

θ	dt	E_∞	E_{RMS}	C_1-order
1	0.1	1.4900*e*-02	1.0400*e*-02	—
	0.05	5.5000*e*-03	3.8000*e*-03	3.3107
	0.01	5.0083*e*-04	3.4937*e*-04	3.4282
	0.005	1.8363*e*-04	1.2741*e*-04	3.3330
	0.001	1.4575*e*-05	9.1709*e*-06	3.6248
$\frac{1}{2}$	0.1	9.0800*e*-02	6.3600*e*-02	—
	0.05	4.3100*e*-02	3.0200*e*-02	2.4753
	0.01	8.0000*e*-03	5.6000*e*-03	2.4094
	0.005	3.9000*e*-03	2.7000*e*-03	2.3867
	0.001	8.3394*e*-04	5.7298*e*-04	2.2069

Table 7: Comparison of E_∞ with [20] for the Problem 4.

α	IS	CNS	[20]
1.15	4.6987*e*-04	9.0819*e*-04	9.1195*e*-04
1.25	4.7856*e*-04	9.3809*e*-04	9.0865*e*-04
1.5	4.9736*e*-04	9.7102*e*-04	8.9931*e*-04

where

$$\mathbb{M}_1 = a_\alpha \mathbf{A} + \theta \mathfrak{L}(\mathbf{A}),$$

$$\mathbb{P} = -a_\alpha \mathbf{A} \lambda^{n-1},$$

$$\mathbb{G}^{n+1} = \mathbb{G}_1^{n+1} + \mathbb{G}_2^{n+1},$$

$$\mathbb{G}_1^{n+1} = \left\{ g_1^{n+1}, 0, \cdots, g_2^{n+1} \right\},$$

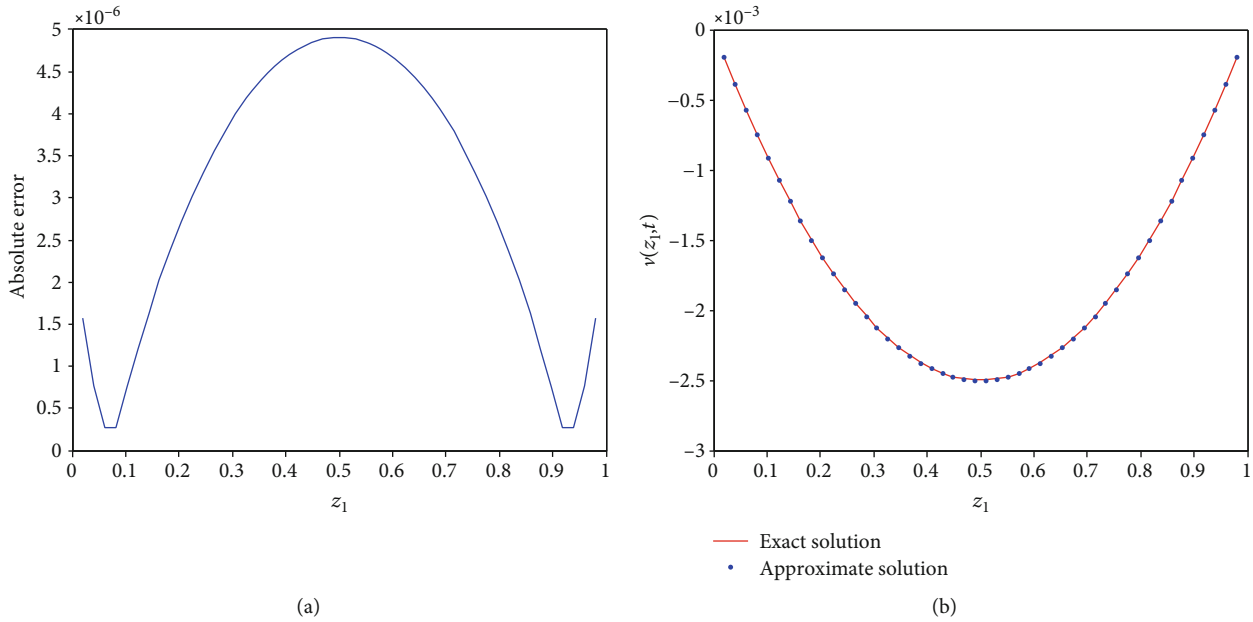

(a) (b)

FIGURE 8: (a) E_{abs} (b) exact and approximate solution for $\alpha = 1.15$ for the Problem 6.

$$\mathbb{G}_2^{n+1} = -2a_\alpha b_n\left(v^1 - v^0 - dtv_t^0\right) - a_\alpha \sum_{k=1}^{n-1} b_k\left(v^{n-k+1} - 2v^{n-k} + v^{n-k-1}\right) + \psi^{n+1}. \quad (44)$$

We can use Eq. (41) and Eq. (43) to find the solution at any time level t^n for $n \geq 1$.

4. Numerical Results

This section is devoted to the numerical implementation of the schemes constructed in Section 2 and Section 3. We have applied schemes over six problems including one-dimensional and two-dimensional time-fractional PDEs. Problems with different types of domains and geometries are also included. We assess the accuracy of the method by taking different values of t and α. We have utilized the following error norms:

$$E_{\text{abs}} = |\widehat{v}(i) - v(i)|, \qquad i = 1, 2, \cdots, N,$$
$$E_\infty = \max |\widehat{v}(i) - v(i)|,$$
$$E_{\text{RMS}} = \sqrt{\left(\frac{1}{N}\sum_{i=1}^{N} {E_{\text{abs}}}^2\right)}. \quad (45)$$

Computational orders for time and space are calculated, respectively, by the formula,

$$C_1 - \text{order} = \frac{\log\left(E_\infty(dt_1)/E_\infty(dt_2)\right)}{\log\left(dt_1/dt_2\right)},$$
$$C_2 - \text{order} = \frac{\log\left(E_\infty(dx_1)/E_\infty(dx_2)\right)}{\log\left(dx_1/dx_2\right)}. \quad (46)$$

Figures are incorporated to show the performance of the method. We have applied IS and CNS and have compared the results. An attempt is made to apply the schemes for some nonuniform nodes including Chebyshev, random, Halton, and scattered data nodes. Also, numerical simulation is performed for some irregular domains. Moreover, we have compared our results with the results reported in [28, 44]. Convergence order is calculated in all the problems, and there is uniform convergence in all the problems.

$$\frac{\partial^\alpha v}{\partial t^\alpha} - \frac{\partial^2 v}{\partial z_1^2} = \psi(z_1, t), 0 \leq z_1 \leq 1, 0 < \alpha < 1, t > 0, \quad (47)$$

where

$$\psi(z_1, t) = \frac{2}{\Gamma(3-\alpha)}\left(t^{2-\alpha}\sin\left(2\pi z_1\right)\right) + 4\pi^2 t^2 \sin\left(2\pi z_1\right), \quad (48)$$

with the exact solution

$$v(z_1, t) = t^2 \sin\left(2\pi z_1\right). \quad (49)$$

Problem 3. In the first problem, we take the following time-fractional *PDE* [23].

IC is given as $v(z_1, 0) = 0$ with homogeneous BCs. In Figure 1, E_∞ is plotted for different values of α. It can be observed that increasing value of α causes less accuracy of results. Also, it is clear that IS gives more accurate results than CNS. Figure 2 displays exact/approximate solution and absolute error at $t = 1, c = 5.1$, and $dt = 0.001$. In Figure 3, numerical solutions at different time levels are plotted. Table 1 is concerned with the convergence order,

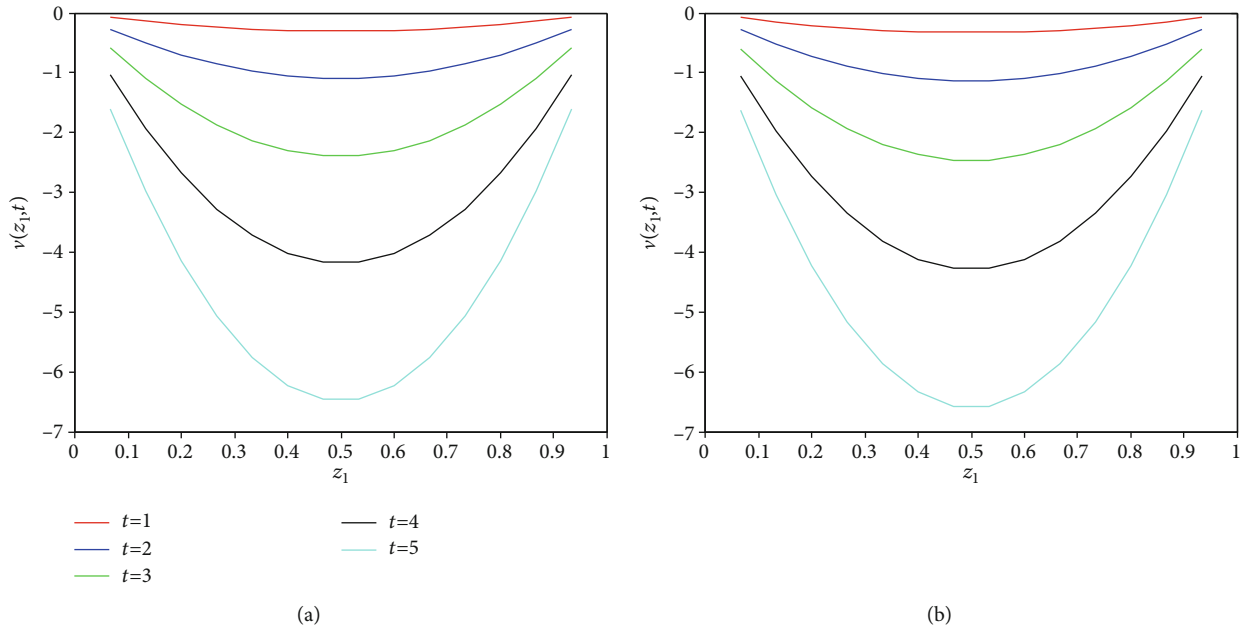

Figure 9: Approximate solution at different time levels by using (a) IS and (b) CNS for Problem 4.

Table 8: Error norms at $t = 1$ for different time steps with $c = 5.9$, $N = 50$ for the Problem 4.

θ	dt	E_∞	E_{RMS}	C_1 − order
1	0.1	5.2500e-02	3.8000e-02	—
	0.05	2.5600e-02	1.8500e-02	1.0362
	0.01	5.0000e-03	3.6000e-03	1.0147
	0.005	2.5000e-03	1.8000e-03	1.0000
	0.001	1.2000e-03	8.9473e-04	0.4560
$\frac{1}{2}$	0.1	7.7300e-02	5.5900e-02	—
	0.05	3.7400e-02	2.7100e-02	1.0474
	0.01	7.3000e-03	5.3000e-03	1.0151
	0.005	3.7000e-03	2.7000e-03	0.9804
	0.001	9.6490e-04	7.0544e-04	0.8351

Table 9: Error norms and computational order for different dx with $c = 100$, $\alpha = 1.5$, and $t = 0.1$ for the Problem 4.

θ	dx	E_∞	E_{RMS}	C_2-order
1	0.1	2.1000e-03	1.5000e-03	—
	0.05	1.7000e-03	1.2000e-03	0.3049
	0.01	4.0345e-04	3.2477e-04	0.8937
	0.005	1.3119e-04	1.1574e-04	1.6207
	0.001	4.8815e-05	3.5377e-05	0.6143
$\frac{1}{2}$	0.1	2.1000e-03	1.5000e-03	—
	0.05	1.7000e-03	1.2000e-03	0.3049
	0.01	3.9522e-04	3.1891e-04	0.9065
	0.005	1.2686e-04	1.1204e-04	1.6394
	0.001	5.0791e-05	3.7090e-05	0.5687

and it shows that the scheme is convergent as proved theoretically. In Table 2, we have computed the numerical results utilizing the IS and the CNS for various values of α's. It is observed from the table that the IS produced better results as compared to CNS.

$$\frac{\partial^\alpha v}{\partial t^\alpha} - \frac{\partial^2 v}{\partial z_1^2} + v = \psi(z_1, t), 0 \le z_1 \le 1, 0 < \alpha < 1, t > 0, \quad (50)$$

where

$$\psi(z_1, t) = \Gamma(2+\alpha) e^{z_1} t, \quad (51)$$

with the exact solution

$$v(z_1, t) = e^{z_1} t^{1+\alpha}, \quad (52)$$

where IC is considered as $v(z_1, 0) = 0$ while the BCs are $v(0, t) = t^{1+\alpha}$, $v(1, t) = et^{1+\alpha}$. In Table 3, IS and CNS are compared with collocation finite element scheme (CFES) [44] which indicates the admirable performance of both the schemes. Figure 4 shows the behaviour of IS scheme by plotting absolute error and approximate/exact solution. One can examine that error decays with increasing x. In Figure 5, we have plotted numerical results for different values of t. Convergence order is calculated in Table 4, and the uniform convergence is obtained.

$$\frac{\partial^\alpha v}{\partial t^\alpha} - \frac{\partial^2 v}{\partial z_1^2} - v = \psi(z_1, t), \quad 0 \le z_1 \le \pi, 0 < \alpha < 1, t > 0, \quad (53)$$

where

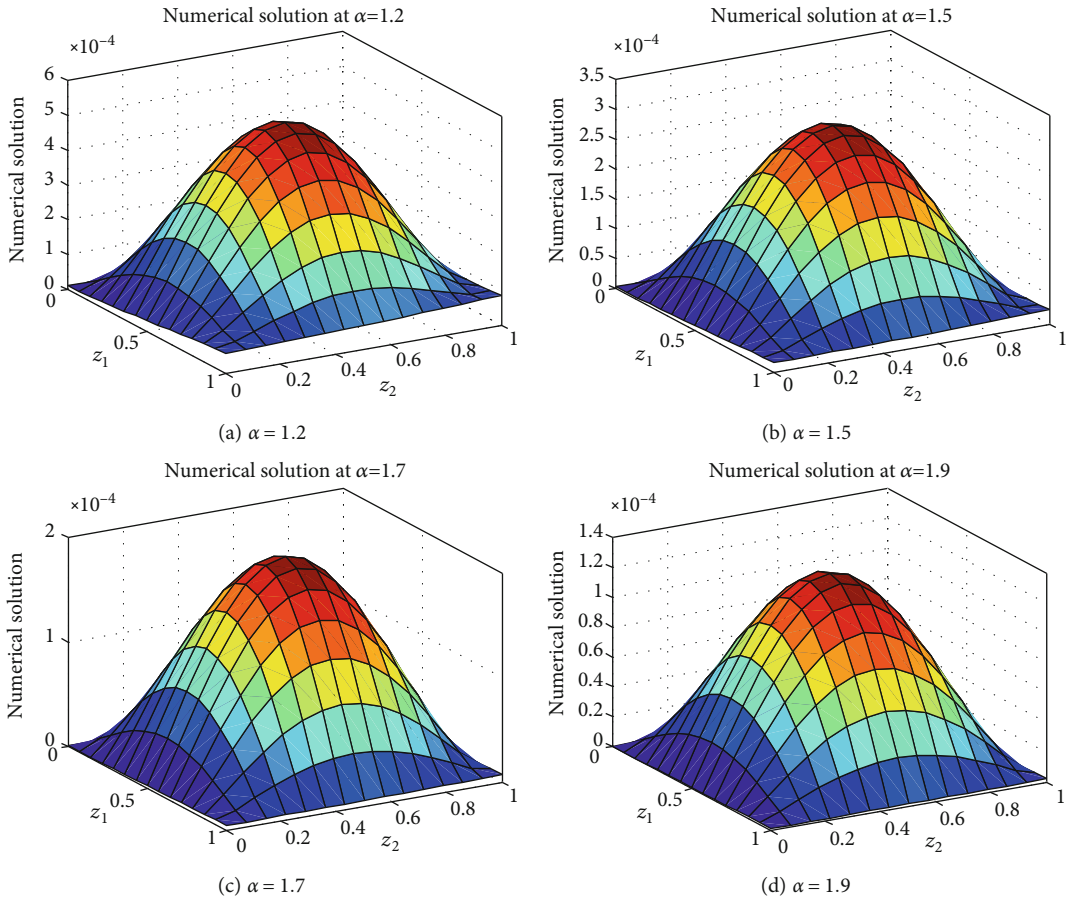

(a) $\alpha = 1.2$ (b) $\alpha = 1.5$

(c) $\alpha = 1.7$ (d) $\alpha = 1.9$

FIGURE 10: Approximate solution for different values of α for the Problem 7.

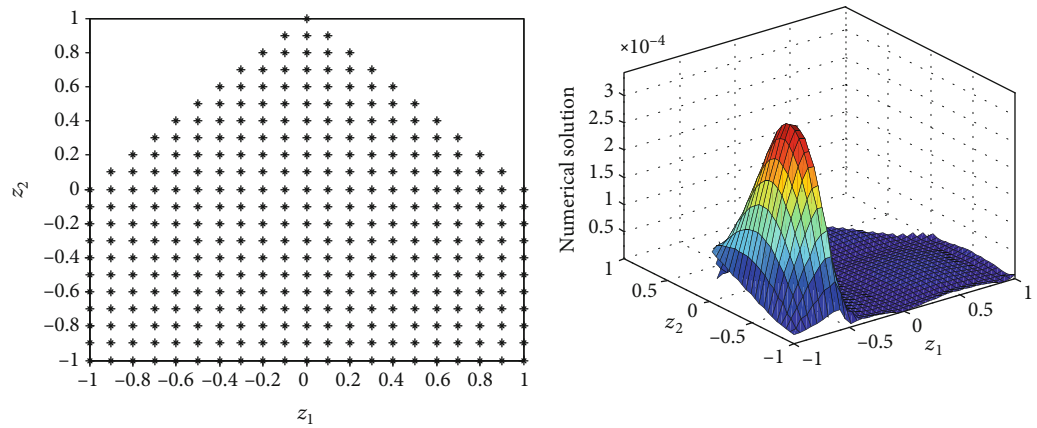

(a) (b)

FIGURE 11: (a) Irregular domain and (b) absolute error for Problem 7.

$$\psi(z_1, t) = \frac{2}{\Gamma(3-\alpha)} t^{2-\alpha} \sin(z_1), \tag{54}$$

with the exact solution

$$\nu(z_1, t) = t^2 \sin(z_1). \tag{55}$$

Problem 4. We consider the following problem [44].

Problem 5. In this problem, we take the following time-fractional PDE [44]

IC is $\nu(z_1, 0) = 0$ and with BCs $\nu(0, t) = 0, \nu(\pi, t) = 0$. Table 5 shows the performance of IS, CNS, and CFES. One can see that IS and CNS give less error than CFES. Figure 6 is aimed at showing absolute error and exact and approximate solution for $\alpha = 0.20$. We can inspect that results obtained from IS scheme agree with that obtained from the

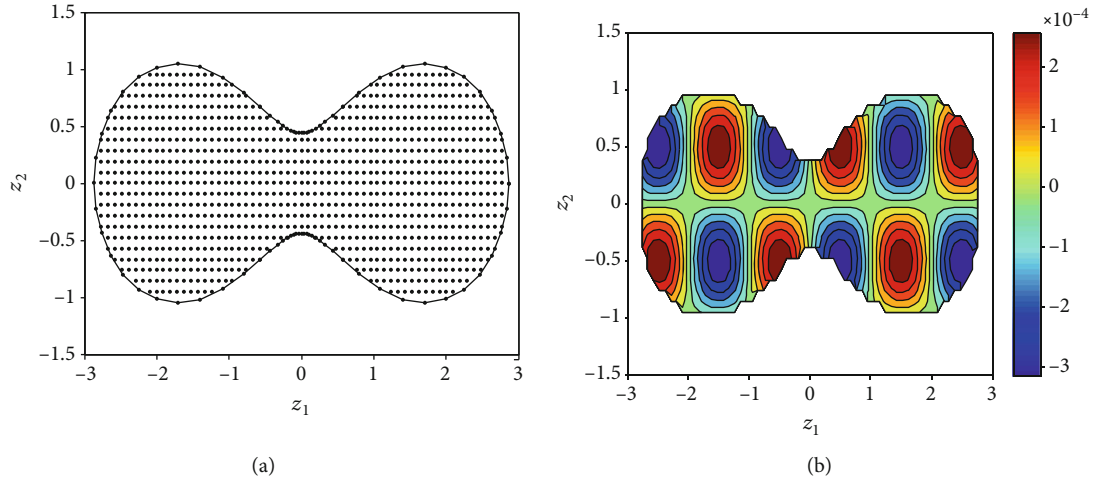

Figure 12: (a) Irregular domain and (b) numerical solution for the Problem 7.

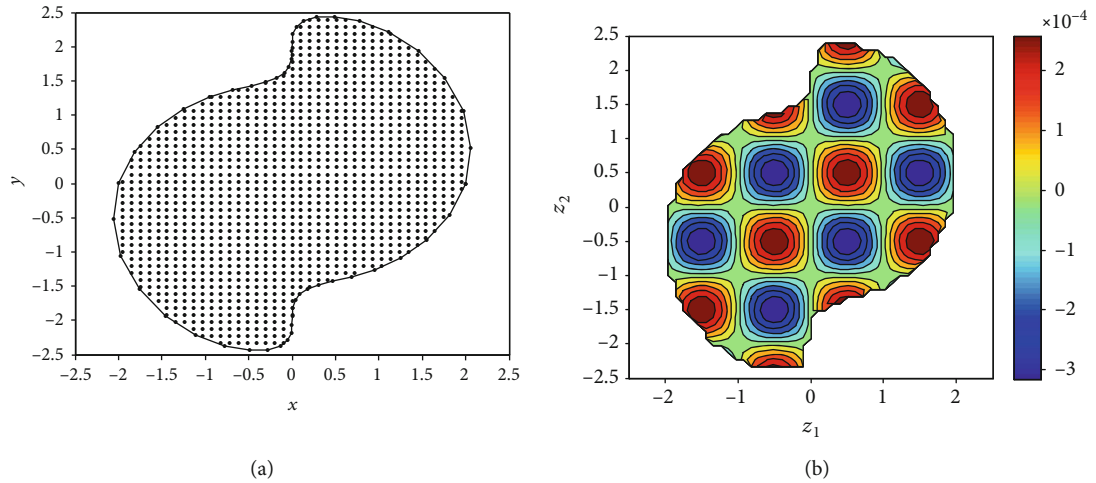

Figure 13: (a) Irregular domain and (b) numerical solution for the Problem 7.

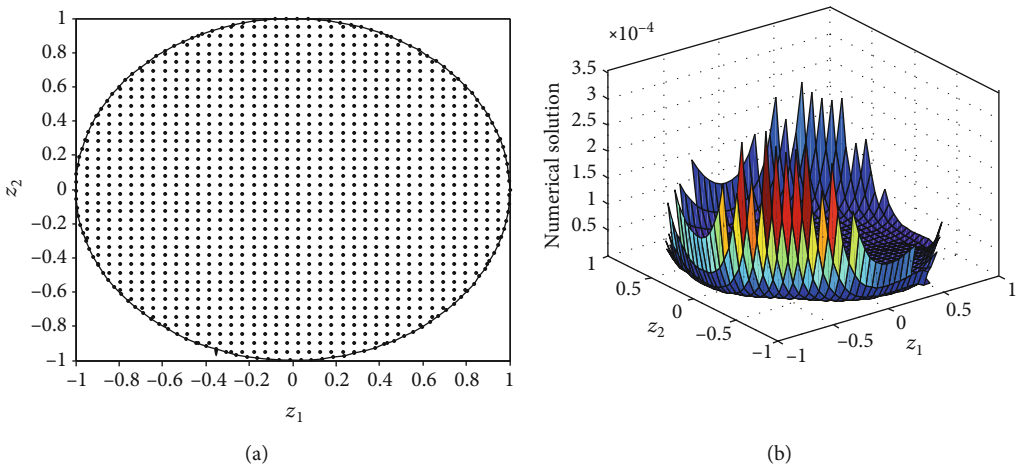

Figure 14: (a) Irregular domain and (b) absolute error for Problem 7.

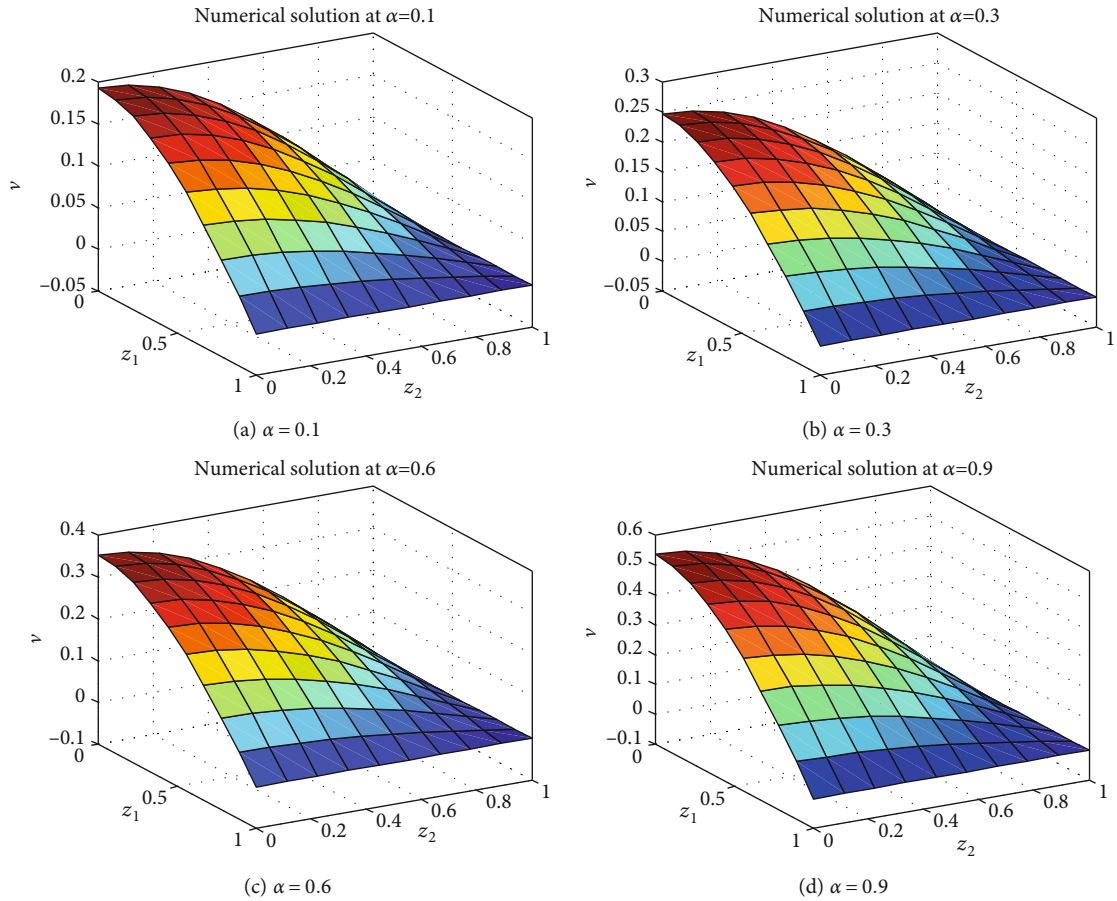

(a) $\alpha = 0.1$ (b) $\alpha = 0.3$

(c) $\alpha = 0.6$ (d) $\alpha = 0.9$

FIGURE 15: Approximate solution for different values of α for the Problem 8.

exact solution. Figure 7 concerns with the numerical solution at different time levels. In Table 6, the order of convergence is calculated which shows the convergence of scheme.

$$\frac{\partial^\alpha v}{\partial t^\alpha} - \frac{\partial^2 v}{\partial z_1^2} = \psi(z_1, t), 0 \le z_1 \le 1, 1 < \alpha < 2, t > 0, \quad (56)$$

where

$$\psi(z_1, t) = \frac{2t^{2-\alpha}}{\Gamma(3-\alpha)} z_1(z_1 - 1) - 2t^2, \quad (57)$$

with the exact solution

$$v(z_1, t) = t^2 z_1(z_1 - 1). \quad (58)$$

Problem 6. In this problem, we take $\mathfrak{L}(v) = -\partial^2 v/\partial z_1^2$ [28] and consider

ICs are given by $v(z_1, 0) = 0, v_t(z_1, 0) = 0$ and with BCs $v(0, t) = 0, v(1, t) = 0$. In Table 7, E_∞ error norm is given for IS, CNS, and meshless Galerkin method (MGM) [28]. We can see that IS produces more accurate results than both CNS and MGM. Figure 8 displays E_{abs} and relationship between exact and numerical solution. Figure 9 is devoted to plot solution at different time levels. In Tables 8 and 9, convergence orders are calculated in time and space, respectively. It can be seen that the method is uniformly convergent in time as well as space.

$$\frac{\partial^\alpha v}{\partial t^\alpha} = \left(\frac{\partial^2 v}{\partial z_1^2} + \frac{\partial^2 v}{\partial z_2^2}\right) + \psi(z_1, z_2, t), \Omega = [0, 1] \times [0, 1], 1 < \alpha < 2, t \in (0, 1], \quad (59)$$

where

$$\psi(z_1, z_2, t) = \sin(\pi z_1) \sin(\pi z_2) \left[\frac{\Gamma(3+\alpha)}{2} t^2 + 2t^{2+\alpha}\right], \quad (60)$$

and the exact solution is

$$v = t^{2+\alpha} \sin(\pi z_1) \sin(\pi z_2), \quad (61)$$

with the ICs

$$v(z_1, z_2, t) = 0, v_t(z_1, z_2, t) = 0, (z_1, z_2) \in \Omega, t = 0 \quad (62)$$

and the BCs

$$v(z_1, z_2, t) = t^{2+\alpha} \sin(\pi z_1) \sin(\pi z_2), (z_1, z_2) \in \partial\Omega. \quad (63)$$

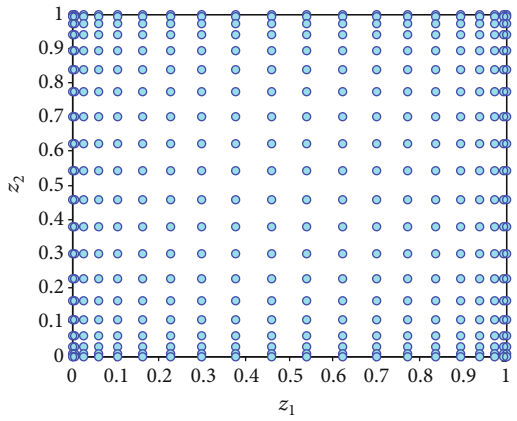

(a) Chebyshev nodes

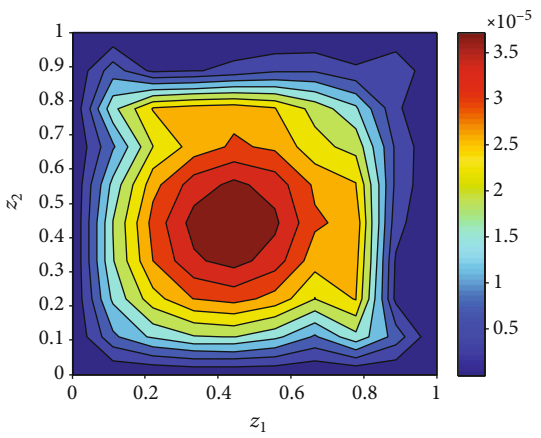

(b) E_∞ using Chebyshev nodes

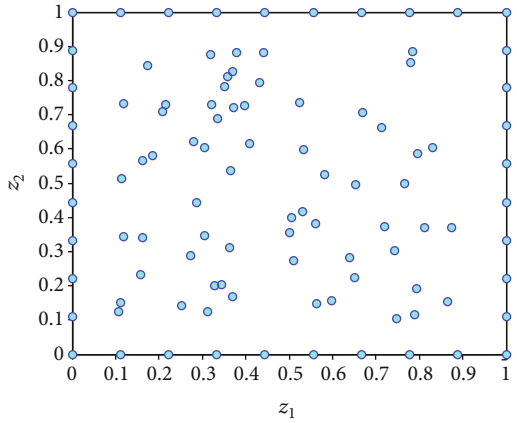

(c) Random nodes

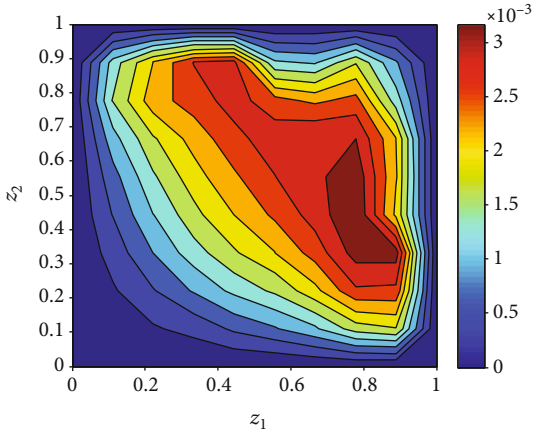

(d) E_∞ using random nodes

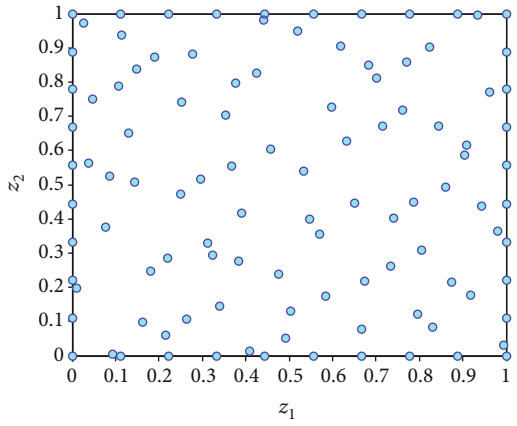

(e) Halton nodes

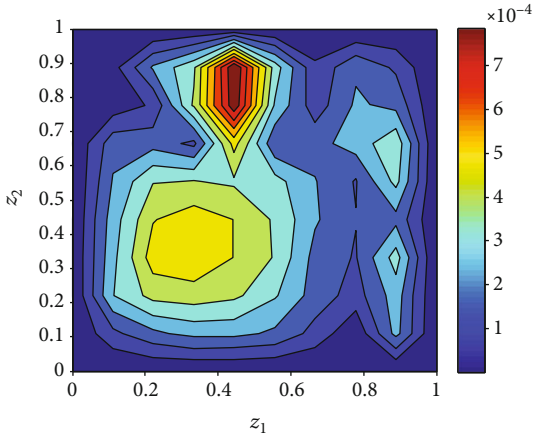

(f) E_∞ using Halton nodes

Figure 16: Continued.

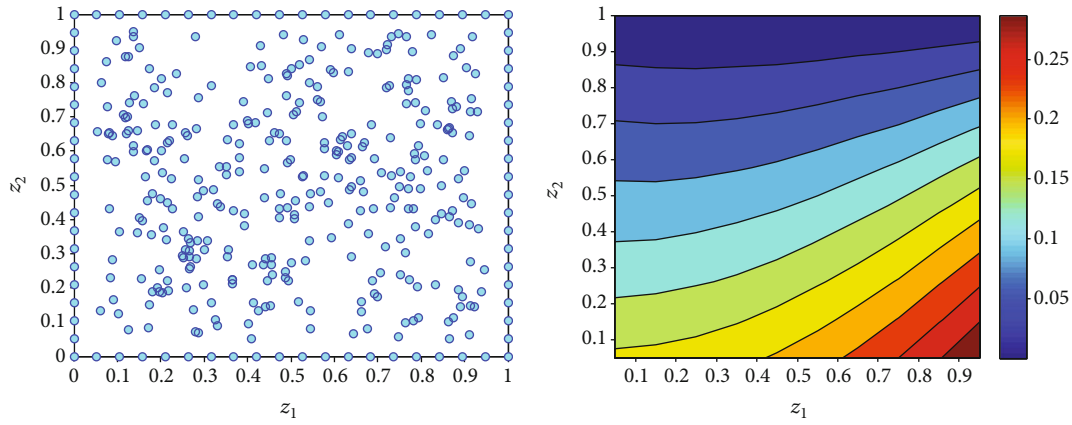

(g) Scattered data nodes

(h) E_∞ using scattered data nodes

FIGURE 16: E_∞ with different nonuniform nodes for the Problem 8.

Problem 7. In this problem, two-dimensional time fractional diffusion-wave equation [(40)] is considered

In this problem, we have taken $c = 5.5$, $dt = 0.001$, $T = 0.1$, and $N = 30$. We have plotted approximate solution for uniform nodes and different values of α in Figure 10. Numerical simulation is performed for irregular domains as well. Numerical solution for different types of irregular domains are presented in Figures 11–14. It can be seen that the better approximate solution is achieved for the irregular domain.

$$\frac{\partial^\alpha \nu}{\partial t^\alpha} = \left(\frac{\partial^2 \nu}{\partial z_1^2} + \frac{\partial^2 \nu}{\partial z_2^2}\right), (z_1, z_2) \in \Omega = [0,1] \times [0,1], 0 < \alpha < 1, t \in (0,0.5), \tag{64}$$

with the exact solution

$$\nu(z_1, z_2, t) = E_\alpha\left(-\frac{1}{2}\pi^2 t^\alpha\right) \cos\left(\frac{\pi}{2} z_1\right) \cos\left(\frac{\pi}{2} z_2\right), \tag{65}$$

where Mittag-Leffler function (one parameter) is defined by

$$E_\alpha(\xi) = \sum_{j=0}^{\infty} \frac{\xi^j}{\Gamma(\alpha j + 1)}, \alpha > 0. \tag{66}$$

We consider IC from $\nu(z_1, z_2, 0) = \cos(\pi/2z_1) \cos(\pi/2z_2)$, and the BCs are drawn from the exact solution. We have performed computations for $c = 13$, $t = 1$, $dt = 0.01$, and $N = 30$. In Figure 15, we have given an approximate solution for different values of α for uniform nodes, while in Figure 16, we have plotted E_∞ error norm for different types of nonuniform nodes for $N = 100$. We got reasonable accuracy for these cases as well.

Problem 8. In this problem, we take the following time FPDE [45].

5. Conclusion

In this work, an attempt is made to propose IS and CNS schemes for the solution of time-fractional PDEs. The time derivative is defined and simplified in Caputo sense and then its value is substituted in governing equation along with replacement of space derivatives by RBFs. This paper has an edge over the existing papers in the sense that in this paper, the scheme is constructed for $0 < \alpha < 1$ and $1 < \alpha < 2$ and for IS and CNS. Problems are given to show the behaviour of the method. Numerical results for different values of α are demonstrated to examine the effect of α over solution. Results produced by IS are compared with that by CNS. Results are also compared with some other methods in the literature. This comparison clearly indicates the impressive performance of our schemes. In order to utilize the advantage of RBF collocation method for nonuniform nodes and irregular domain, numerical simulation is performed and remarkable results are achieved for nonuniform nodes and irregular domain.

Data Availability

Data will be available on request.

Conflicts of Interest

The authors declare that there are no conflicts of interest associated with this publication.

Acknowledgments

The research was supported by the National Natural Science Foundation of China (Grant No. 11501170). The first author is grateful to Shaheed Benazir Bhutto Women University Peshawar, Pakistan, for study leave.

References

[1] I. Ahmad, H. Ahmad, P. Thounthong, Y.-M. Chu, and C. Cesarano, "Solution of multi-term time-fractional PDE

models arising in mathematical biology and physics by local meshless method," *Symmetry*, vol. 12, no. 7, p. 1195, 2020.

[2] I. Ahmad, M. N. Khan, M. Inc, H. Ahmad, and K. S. Nisar, "Numerical simulation of simulate an anomalous solute transport model via local meshless method," *Alexandria Engineering Journal*, vol. 59, no. 4, pp. 2827–2838, 2020.

[3] M. Inc, M. N. Khan, I. Ahmad, S.-W. Yao, H. Ahmad, and P. Thounthong, "Analysing time-fractional exotic options via efficient local meshless method," *Results in Physics*, vol. 19, article 103385, 2020.

[4] A. Kumar, H. V. S. Chauhan, C. Ravichandran, K. S. Nisar, and D. Baleanu, "Existence of solutions of non-autonomous fractional differential equations with integral impulse condition," *Advances in Difference Equations*, vol. 2020, no. 1, 14 pages, 2020.

[5] H. Ahmad, T. A. Khan, I. Ahmad, P. S. Stanimirović, and Y. M. Chu., "Numerical simulation of simulate an anomalous solute transport model via local meshless method," *Results in Physics*, vol. 19, article 103462, 2020.

[6] M. H. Srivastava, H. Ahmad, I. Ahmad, P. Thounthong, and N. M. Khan, "Numerical simulation of three-dimensional fractional-order convection-diffusion PDEs by a local meshless method," *Thermal Science*, p. 210, 2020.

[7] N. Valliammal, C. Ravichandran, and K. S. Nisar, "Solutions to fractional neutral delay differential nonlocal systems," *Chaos, Solitons & Fractals*, vol. 138, article 109912, 2020.

[8] M. Arif, F. Ali, I. Khan, and K. S. Nisar, "A time fractional model with non-singular kernel the generalized couette flow of couple stress nanofluid," *IEEE Access*, vol. 8, pp. 77378–77395, 2020.

[9] I. Podulbny, *Fractional Differential Equations*, Academic Press, New York, 1999.

[10] M. M. Raja, V. Vijayakumar, and R. Udhayakumar, "Results on the existence and controllability of fractional integro-differential system of order 1< r<2 via measure of noncompactness," *Chaos, Solitons & Fractals*, vol. 139, article 110299, 2020.

[11] R. Bagley and P. Torvik, "A theoretical basis for the application of fractional calculus to viscoelasticity," *Journal of Rheology*, vol. 27, no. 3, pp. 201–210, 1983.

[12] D. Baleanu, K. Diethelm, E. Scalas, and J. J. Trujillo, "Fractional Calculus Models and Numerical Methods," in *Series on complexity, nonlinearity and chaos*, World Scientific, Boston, 2012.

[13] K. Diethelm and N. J. Ford, "Analysis of fractional differential equations," *Journal of Mathematical Analysis and Applications*, vol. 265, no. 2, pp. 229–248, 2002.

[14] W. Wyss, "The fractional diffusion equation," *Journal of Mathematical Physics*, vol. 27, no. 11, pp. 2782–2785, 1986.

[15] I. Ahmad, M. Siraj-ul-Islam, and S. Zaman, "Local meshless differential quadrature collocation method for time-fractional PDEs," *Discrete & Continuous Dynamical Systems – S*, vol. 13, no. 10, pp. 2641–2654, 2020.

[16] A. Saadatmandi and M. Dehghan, "A new operational matrix for solving fractional-order differential equations," *Computers & Mathematcs with Applications*, vol. 59, no. 3, pp. 1326–1336, 2010.

[17] C. Ravichandran, K. Logeswari, S. K. Panda, and K. S. Nisar, "On new approach of fractional derivative by Mittag-Leffler kernel to neutral integro-differential systems with impulsive conditions," *Chaos, Solitons & Fractals*, vol. 139, article 110012, 2020.

[18] N. A. Sheikh, M. Jamil, D. L. C. Ching, I. Khan, M. Usman, and K. S. Nisar, "A generalized model for quantitative analysis of sediments loss: a Caputo time fractional model," *Journal of King Saud University-Science*, 2020.

[19] R. Subashini, C. Ravichandran, K. Jothimani, and H. M. Baskonus, "Existence results of Hilfer integro-differential equations with fractional order," *Discrete & Continuous Dynamical Systems-S*, vol. 13, no. 3, pp. 911–923, 2020.

[20] S. B. Yuste and L. Acedo, "An explicit finite difference method and a new Von Neumann-type stability analysis for fractional diffusion equations," *SIAM Journal on Numerical Analysis*, vol. 42, no. 5, pp. 1862–1874, 2005.

[21] O. P. Agrawal, "Solution for a fractional diffusion-wave equation defined in a bounded domain," *Nonlinear Dynamics*, vol. 29, no. 1/4, pp. 145–155, 2002.

[22] F. Liu, V. Anh, I. Turner, and P. Zhuang, "Time fractional advection-dispersion equation," *Journal of Applied Mathematics and Computing*, vol. 13, no. 1-2, pp. 233–245, 2003.

[23] Y. Jiang and J. Ma, "High-order finite element methods for time-fractional partial differential equations," *Journal of Computational and Applied Mathematics*, vol. 235, no. 11, pp. 3285–3290, 2011.

[24] A. Chang, H. Sun, C. Zheng et al., "A Time Fractional Convection-Diffusion Equation to Model Gas Transport through Heterogeneous Soil and Gas Reservoirs," *Physica A: Statistical Mechanics and its Applications*, vol. 502, pp. 356–369, 2018.

[25] I. Ahmad, H. Ahmad, A. E. Abouelregal, P. Thounthong, and M. Abdel-Aty, "Numerical study of integer-order hyperbolic telegraph model arising in physical and related sciences," *The European Physical Journal Plus*, vol. 135, no. 9, pp. 1–14, 2020.

[26] I. Ahmad, M. Riaz, M. Ayaz, M. Arif, S. Islam, and P. Kumam, "Numerical simulation of partial differential equations via local meshless method," *Symmetry*, vol. 11, no. 2, article 257, 2019.

[27] M. N. Khan, I. H. Siraj-ul-Islam, I. Ahmad, and H. Ahmad, "A local meshless method for the numerical solution of space-dependent inverse heat problems," *Mathematical Methods in the Applied Sciences*, 2020.

[28] M. Dehghan, M. Abbaszadeh, and A. Mohebbi, "Analysis of a meshless method for the time fractional diffusion-wave equation," *Numerical algorithms*, vol. 73, no. 2, pp. 445–476, 2016.

[29] M. Nawaz, I. Ahmad, and H. Ahmad, "A radial basis function collocation method for space-dependent inverse heat problems," *Journal of Applied and Computational Mechanics*, 2020.

[30] Q. Liu, F. Liu, I. Turner, V. Anh, and Y. T. Gu, "A RBF meshless approach for modeling a fractal mobile/immobile transport model," *Applied Mathematics and Computation*, vol. 226, pp. 336–347, 2014.

[31] Q. Liu, Y. Zhuang, P. Liu, and Y. Nie, "An implicit, RBF meshless approach for time fractional diffusion equations," *Computational Mechanics*, vol. 48, no. 1, pp. 1–12, 2011.

[32] P. Thounthong, M. N. Khan, I. Hussain, I. Ahmad, and P. Kumam, "Symmetric radial basis function method for simulation of elliptic partial differential equations," *Mathematics*, vol. 6, no. 12, p. 327, 2018.

[33] F. Usta, "Numerical solution of fractional elliptic PDEs by the collocation method," *Applications and Applied Mathematics*, vol. 12, pp. 470–478, 2017.

[34] W. Chen, L. Ye, and H. Sun, "Fractional diffusion equations by the Kansa method," *Computers & Mathematcs with Applications*, vol. 59, no. 5, pp. 1614–1620, 2010.

[35] Y. T. Gu, P. Zhuang, and F. Liu, "An advanced implicit meshless approach for the non-linear anomalous subdiffusion equation," *International Journal of Computational Methods*, vol. 56, pp. 303–334, 2010.

[36] E. J. Kansa, "Multiquadrics—a scattered data approximation scheme with applications to computational fluid-dynamics—II solutions to parabolic, hyperbolic and elliptic partial differential equations," *Computers & Mathematics with Applications*, vol. 19, no. 8-9, pp. 147–161, 1990.

[37] C. S. Huang, C. F. Lee, and A. H. D. Cheng, "Error estimate, optimal shape factor, and high precision computation of multiquadric collocation method," *Engineering Analysis with Boundary Elements*, vol. 31, no. 7, pp. 614–623, 2007.

[38] C. S. Huang, H. D. Yen, and A. H. D. Cheng, "On the increasingly flat radial basis function and optimal shape parameter for the solution of elliptic PDEs," *Engineering Analysis with Boundary Elements*, vol. 34, no. 9, pp. 802–809, 2010.

[39] S. Rippa, "An algorithm for selecting a good value for the parameter c in radial basis function interpolation," *Advances in Computational Mathematics*, vol. 11, no. 2/3, pp. 193–210, 1999.

[40] G. R. Liu and Y. T. Gu, "A point interpolation method for two-dimensional solids," *International Journal for Numerical Methods in Engineering*, vol. 50, pp. 221–236, 2001.

[41] G. E. Fasshauer, *Meshfree Aprooximation Methods with Matlab*, Word Scientific Publishing Co. Pte. Ltd, 2007.

[42] H. Wendland, *Scattered Data Approximation*, Cambridge University Press, Cambridge Monographs on Applied and Computational Mathematics, 2010.

[43] H. Wendland, "Local polynomial reproduction and moving least squares approximation," *IMA Journal of Numerical Analysis*, vol. 21, no. 1, pp. 285–300, 2001.

[44] Y. Ucar, N. M. Yagmurlu, O. Tasbozan, and A. Esen, "Numerical solution of some fractional partial differential equations using collocation finite element method," *Progress in Fractional Differentiation and Applications*, vol. 1, pp. 157–164, 2015.

[45] A. Shirzadi, L. Ling, and S. Abbasbandy, "Meshless simulations of the two-dimensional fractional-time convection-diffusion-reaction equations," *Engineering Analysis with Boundary Elements*, vol. 36, no. 11, pp. 1522–1527, 2012.